



# Multi-satellite Capture Configuration with Continuous Thrust

Weike Wang<sup>1,2</sup> · Hanjun Wang<sup>1</sup> · Tian Liao<sup>1</sup> · Shunli Li<sup>1</sup> · Mengping Zhu<sup>2</sup>

Received: 5 May 2024 / Revised: 20 June 2024 / Accepted: 4 July 2024  
© Chinese Society of Astronautics 2024

## Abstract

The pursuit-evasion game of orbital satellite is an important research problem in the field of space security. In this pursuit-evasion game, intercepting the target usually requires superior maneuvering capabilities. To address this issue, a method is proposed in this paper to use multiple small satellites with weaker maneuvering capabilities to encircle and capture larger targets with stronger maneuvering abilities. Firstly, based on Tsiolkovsky's formula, the planar interception problem is derived and a one-on-one planar interception strategy is designed. Next, the existence of solutions for planar mission is analyzed, and a multi-satellite encirclement configuration is designed based on elliptical passive flyby theory. Finally, simulation analysis is conducted on the impact of various design parameters of the planar interception configuration on the encirclement task. The results indicate that the initial distance between interceptor and target significantly affects interception time. Simulation results validate that the proposed interception strategy and encirclement configuration can achieve rapid interception of close-range targets effectively.

**Keywords** Pursuit-evasion game · Capture configuration design · Continuous thrust · Interception strategy

## 1 Introduction

The rapid development of space exploration and aerospace technology has brought significant changes to daily life, while also exerting a crucial impact on conflicts and security worldwide. In recent years, an increasing number of researchers have begun to focus on the study of orbital

satellite pursuit-evasion games [1, 2]. Existing research on satellite pursuit-evasion games is mostly based on differential game theory [3–7], often involving one-on-one interception scenarios where the interceptor's maneuverability typically surpasses that of the target. Some researchers [8, 9] have also delved into pursuit-evasion games involving incomplete information in the context of orbital satellite maneuvering.

Several studies have initially explored pursuit-evasion problems involving multiple satellites. Zhou Junfeng [10] designed a tracker combination objective function based on fuzzy comprehensive evaluation, establishing a "pursue-evade-defend" model for satellite under continuous thrust. Chen Musheng [11] created pursuit-evasion strategy models for scenarios such as "two pursuers against one evader" and "one pursuer against one evader with defense" based on differential game theory, utilizing cooperative evolution algorithms for solving. Liu et al. [12] explored the pursuit-evasion problem of three-dimensional orbital satellite utilizing a hybrid methodology that integrates particle swarm optimization with the Newton interpolation algorithm. Moreover, in recent years, machine learning techniques have been employed in the design of satellite control studies [13]. Some researchers have applied reinforcement learning methods in satellite pursuit-evasion games [14, 15], which have already found application in multi-drone cooperative tasks

---

Weike Wang and Hanjun Wang contributed equally to this work.

---

✉ Shunli Li  
lishunli@hit.edu.cn

Weike Wang  
wangwk@stu.hit.edu.cn

Hanjun Wang  
Whj\_Hit@outlook.com

Tian Liao  
liaotian@stu.hit.edu.cn

Mengping Zhu  
zhumengping@qxslab.cn

<sup>1</sup> School of Astronautics, Harbin Institute of Technology, 92 Xidazhi Street, Harbin 150001, Heilongjiang, People's Republic of China

<sup>2</sup> Qian Xuesen Laboratory of Space Technology, China Academy of Space Technology, 104 Youyi Road, Beijing 100094, People's Republic of China

[16, 17]. Moreover, Zhao et al. [18] proposed a comprehensive problem model for the multi-constrained impulse-based orbital pursuit-evasion game and enhanced the Multi-Agent Deep Deterministic Policy Gradient (MADDPG) algorithm to enable intelligent training and solution exploration for pursuit-evasion strategies in impulse-based orbital maneuvers. These research achievements serve as references for studying collaborative confrontations among multiple satellite.

Inspired by the Starlink and SAR (synthetic aperture radar) satellite constellations, when facing large satellite with strong maneuverability capabilities, it is possible to employ multiple smaller satellites with weaker maneuverability to encircle and capture the target effectively. This ensures that regardless of the direction in which the target maneuvers, at least one small satellite can intercept it after a certain period of continuous propulsion. The long-term velocity accumulation achievable through low-thrust thrusters compensates for the weaker maneuvering abilities of small satellites. Currently, there is relatively limited research on multi-satellite encirclement configuration design; moreover, due to non-compliance with Keplerian orbits under continuous propulsion methods [10], dynamic modeling becomes more complex when designing encirclement configurations using this mode of movement.

This paper focuses on large impulse-maneuvered satellites in GSO (geostationary orbit) as targets and proposes a method for rapid interception by continuously propelling towards the target satellite. We propose a planar interception problem and design an interception strategy that requires relatively low computational resources, making it more suitable for real-time planning on small satellites. Furthermore, we introduce a novel approach to design passive flyby configurations where multiple small satellites surround the target satellite to achieve swift interception against highly maneuverable targets. Through simulation verification, we explore how various parameters affect the effectiveness of the multi-satellite encirclement strategy proposed in this paper, providing insights into its practical applications and potential for enhancing interception capabilities in space operations.

## 2 Fundamental Theory of Planar Interception Problems

### 2.1 Description and Assumptions of the Planar Interception Problem

The results of configuration design are closely related to the maneuvering strategies adopted by the intercepting satellite. Given the complexity of the dynamics model with continuous thrust, simplification is necessary for effective configuration design. In this section, we propose a simplified approach to

planar interception problems and a one-on-one planar interception strategy based on GSO characteristics. The aim is to reduce computational costs in real-time planning for small satellites.

#### 2.1.1 Simplification of Relative Motion Problems in Geostationary Orbit

The relative motion velocity derived from the CW equation in the Hill frame is:

$$\begin{aligned}\dot{x}(t) &= -2\dot{y}(0)\sin\omega t + 2[\dot{x}(0) + 3\omega y(0)] \\ &\quad \times \cos\omega t - [3\dot{x}(0) + 6\omega y(0)] \\ \dot{y}(t) &= \dot{y}(0)\cos\omega t + [2\dot{x}(0) + 3\omega y(0)] \times \sin\omega t\end{aligned}\quad (1)$$

Assuming the target satellite is located in a GSO orbit, which  $\omega$  can be considered negligible, and further assuming that the plane interception time  $t$  is relative to the entire orbital period  $T$ , that is,  $T \gg t$ .

The relative motion velocity in the X–Y plane can then be further simplified as:

$$\begin{aligned}\dot{x}(t) &= \dot{x}(0) \\ \dot{y}(t) &= \dot{y}(0)\end{aligned}\quad (2)$$

That is, the pursuit-evasion problem of short-duration and close-range satellite relative motion in the target satellite GSO orbit can be approximately simplified as uniform rectilinear motion without external forces. It has been verified that for satellites in GSO, when the semi-major axis of the passive elliptical flyby is 20,000m, the error between the relative position vectors of the interceptor and the target, obtained through uniform linear motion and two-body orbital propagation, is less than 100m after 1800s. This level of accuracy is sufficiently small for the design of interception configurations.

#### 2.1.2 Constructing the Interception Problem

Assumption: The problem of relative motion between satellite in close proximity over a short period of time can be approximated as linear motion. As shown in Fig. 1, with the target satellite as the origin, the interception vehicle is stationary relative to the target in a coordinate system at the initial moment. The target satellite moves in a straight line at a constant speed with an initial velocity vector  $v_m$ , where  $\beta$  represents the azimuth angle. At the beginning, the distance between interception vehicle and target is  $R$ , with an azimuth angle  $\alpha$ . The interception vehicle maneuvers using finite thrust, with a constant thrust magnitude of  $F$ , specific impulse of  $I_{sp}$ , and initial mass  $m_0$ . The process of planar interception is illustrated in Fig. 1, involving two maneu-

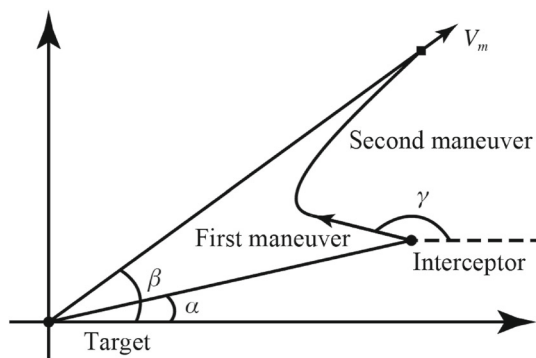


Fig. 1 Demonstration of the planar interception problem

vers to complete the mission. The first maneuver accelerates by changing its azimuth angle  $\gamma$  by an increment of  $\Delta v_1$ ; while for the second maneuver, there is a velocity increment  $\Delta \mathbf{V}_2 = \mathbf{V}_m - \Delta \mathbf{V}_1$  to ensure that at intercept terminal time both position and velocity match for both target and interceptor.

### 2.2 Design of Planar Interception Strategy

In continuous thrust maneuvering, the remaining mass of the interceptor satellite constantly changes as it pursues the target. To further assess the impact of mass variation on the motion of small interceptors, this section analyzes planar interception problems based on Tsiolkovsky’s formula. Additionally, a low-complexity interception strategy suitable for online trajectory planning of small interceptor satellites is designed.

#### 2.2.1 Derivation of Planar Interception Problem Based on Tsiolkovsky’s Formula

The target trajectory is given by:

$$\begin{aligned} x &= t \cdot v_m \cos \beta \\ y &= t \cdot v_m \sin \beta \end{aligned} \tag{3}$$

Initial state of the interceptor satellite:

$$\begin{aligned} x_{0i} &= R \cos \alpha \\ y_{0i} &= R \sin \alpha \end{aligned} \tag{4}$$

Considering two maneuvers based on Tsiolkovsky’s formula leads to a one-dimensional acceleration problem.

The first velocity increment is given by:

$$\Delta \mathbf{V}_1 = \begin{bmatrix} \Delta v_1 \cos \gamma \\ \Delta v_1 \sin \gamma \end{bmatrix} \tag{5}$$

where both  $\Delta v_1$  and  $\gamma$  are unknown quantities.

Displacement during the first acceleration phase:

$$|\Delta \mathbf{S}_1| = \frac{m_0 I_{sp}^2}{F} \left[ 1 - \left( 1 + \frac{|\Delta \mathbf{V}_1|}{I_{sp}} \right) e^{-\frac{|\Delta \mathbf{V}_1|}{I_{sp}}} \right] \tag{6}$$

Corresponding maneuver time:

$$t_a = \frac{m_0 I_{sp}}{F} \left( 1 - e^{-\frac{|\Delta \mathbf{V}_1|}{I_{sp}}} \right) \tag{7}$$

Let the second velocity increment be:

$$\Delta \mathbf{V}_2 = \begin{bmatrix} v_m \cos \beta - \Delta v_1 \cos \gamma \\ v_m \sin \beta - \Delta v_1 \sin \gamma \end{bmatrix} \tag{8}$$

The duration for the second maneuver is:

$$\begin{aligned} t_b &= \frac{m_{d0} I_{sp}}{F} \left( 1 - e^{-\frac{|\Delta \mathbf{V}_2|}{I_{sp}}} \right) \\ &= \frac{m_0 I_{sp}}{F} e^{-\frac{|\Delta \mathbf{V}_1|}{I_{sp}}} \left( 1 - e^{-\frac{|\Delta \mathbf{V}_2|}{I_{sp}}} \right) \end{aligned} \tag{9}$$

Displacement during the second maneuver:

$$\begin{aligned} \Delta \mathbf{S}_2 &= \Delta \mathbf{S}' + \Delta \mathbf{V}_1 \cdot t_b \\ &= |\Delta \mathbf{S}'| \frac{\mathbf{V}_m - \Delta \mathbf{V}_1}{|\mathbf{V}_m - \Delta \mathbf{V}_1|} + \Delta \mathbf{V}_1 \cdot t_b \end{aligned} \tag{10}$$

Here,

$$|\Delta \mathbf{S}'| = \frac{m_0 I_{sp}^2}{F} e^{-\frac{|\Delta \mathbf{V}_1|}{I_{sp}}} \left[ 1 - \left( 1 + \frac{|\Delta \mathbf{V}_2|}{I_{sp}} \right) e^{-\frac{|\Delta \mathbf{V}_2|}{I_{sp}}} \right]$$

Thus, total interception time becomes:

$$\begin{aligned} t &= t_a + t_b + t_g \\ &= \frac{m_0 I_{sp}}{F} \left( 1 - e^{-\frac{|\Delta v_1| + |\Delta v_2|}{I_{sp}}} \right) + t_g \end{aligned} \tag{11}$$

where  $t_a$  and  $t_b$  represent times for the first and second maneuvers respectively;  $t_g$  denotes attitude maneuver time between two maneuvers, which will not be considered in subsequent scenarios for now (i.e.,  $t_g = 0$ ).

Summarizing requirements for planar interception: at time  $t$ , completion of just-in-time finishing for a second maneuver by interceptor satellite where it meets with target satellite with zero relative velocity. Key parameters to focus on include:  $F$  representing interceptor’s maneuvering capability;  $\Delta v_1, \gamma$  representing design parameters for interceptor’s maneuvers;  $R, \alpha$  indicating relative position between interceptor and target satellite;  $t$  denoting interception time.

### 2.2.2 Interception in the Coplanar Pursuit Strategy

For coplanar interception problems, the requirement is to have the target and interceptor satellite meet at the same velocity at the end of the second maneuver at time  $t$ . Following the two-stage interception method described earlier, assuming known initial target velocity, direction, and interceptor's initial position at interception commencement, with design variables being only the magnitude of velocity  $|\Delta v_1|$  at the end of first maneuver and azimuth angle  $\gamma$ .

The position of target satellite at time  $t$  can be obtained by combining equations (3), (7), and (9):

$$\begin{bmatrix} t \cdot v_m \cos \beta \\ t \cdot v_m \sin \beta \end{bmatrix} = \frac{m_0 I_{sp}}{F} \left( 1 - e^{-\frac{|\Delta v_1| + |\Delta v_2|}{I_{sp}}} \right) \times \begin{bmatrix} v_m \cos \beta \\ v_m \sin \beta \end{bmatrix} \tag{12}$$

The position of interceptor satellite at time  $t$  can be derived from Eqs. (6) and (10):

$$\begin{aligned} x_I &= \frac{m_0 I_{sp}^2}{F} \left[ 1 - \left( 1 + \frac{|\Delta \mathbf{V}_1|}{I_{sp}} \right) e^{-\frac{|\Delta \mathbf{V}_1|}{I_{sp}}} \right] \\ &\quad \times \cos \gamma + |\Delta \mathbf{V}_1| \cos \gamma \cdot t_g + \frac{m_0 I_{sp}^2}{F} \\ &\quad \times e^{-\frac{|\Delta \mathbf{V}_1|}{I_{sp}}} \left[ 1 - \left( 1 + \frac{|\Delta \mathbf{V}_2|}{I_{sp}} \right) e^{-\frac{|\Delta \mathbf{V}_2|}{I_{sp}}} \right] \\ &\quad \times \frac{v_m \cos \beta - |\Delta \mathbf{V}_1| \cos \gamma}{\|\Delta \mathbf{V}_2\|} \\ &\quad + \Delta \mathbf{V}_1 \times \cos \gamma \frac{m_0 I_{sp}}{F} e^{-\frac{|\Delta \mathbf{V}_1|}{I_{sp}}} \left( 1 - e^{-\frac{|\Delta \mathbf{V}_2|}{I_{sp}}} \right) \end{aligned} \tag{13}$$

$$\begin{aligned} y_I &= \frac{m_0 I_{sp}^2}{F} \left[ 1 - \left( 1 + \frac{|\Delta \mathbf{V}_1|}{I_{sp}} \right) e^{-\frac{|\Delta \mathbf{V}_1|}{I_{sp}}} \right] \\ &\quad \times \sin \gamma + t_g |\Delta \mathbf{V}_1| \sin \gamma + \frac{m_0 I_{sp}^2}{F} \\ &\quad \times e^{-\frac{|\Delta \mathbf{V}_1|}{I_{sp}}} \left[ 1 - \left( 1 + \frac{|\Delta \mathbf{V}_2|}{I_{sp}} \right) e^{-\frac{|\Delta \mathbf{V}_2|}{I_{sp}}} \right] \\ &\quad \times \frac{v_m \sin \beta - |\Delta \mathbf{V}_1| \sin \gamma}{\|\Delta \mathbf{V}_2\|} \\ &\quad + \Delta \mathbf{V}_1 \sin \gamma \times \frac{m_0 I_{sp}}{F} e^{-\frac{|\Delta \mathbf{V}_1|}{I_{sp}}} \left( 1 - e^{-\frac{|\Delta \mathbf{V}_2|}{I_{sp}}} \right) \end{aligned} \tag{14}$$

Solving the following nonlinear equations will yield design parameters necessary for completing an interception mission:  $\Delta v_1$  and  $\gamma$ :

$$\begin{bmatrix} x_I \\ y_I \end{bmatrix} = \frac{m_0 I_{sp}}{F} \left( 1 - e^{-\frac{|\Delta v_1| + |\Delta v_2|}{I_{sp}}} \right) \times \begin{bmatrix} v_m \cos \beta \\ v_m \sin \beta \end{bmatrix} \tag{15}$$

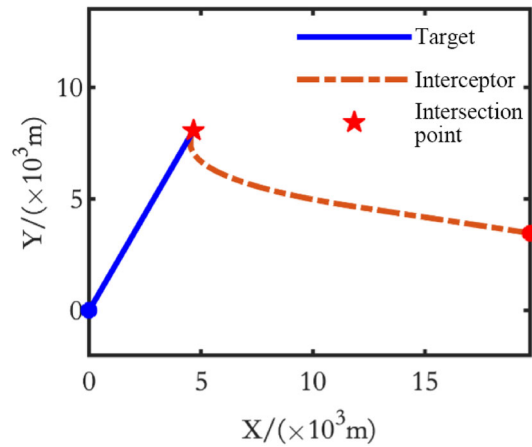


Fig. 2 Interceptor's interception trajectory

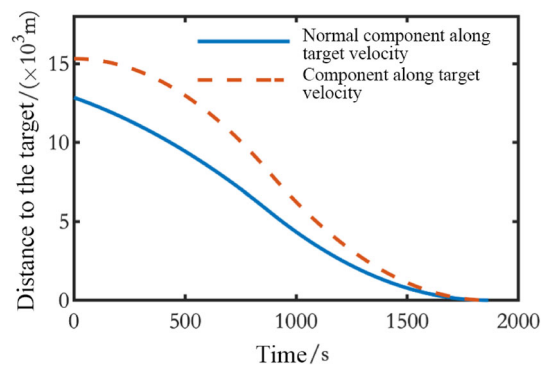


Fig. 3 Distance between the interceptor and the target

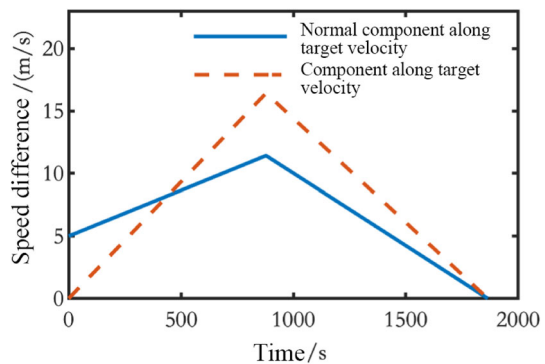


Fig. 4 Speed difference between the interceptor and the target

### 2.2.3 One-on-One Planar Interception Case

To evaluate the interception strategies mentioned above, a simulation is conducted in a one-on-one interception scenario. Assuming the target velocity direction is  $\beta = 30^\circ$ , with a speed of  $v_m = 5m/s$ , and the interceptor has zero initial velocity, starting at a distance of  $R = 20,000m$  from the target, azimuth angle  $\alpha = 10^\circ$ , coasting time  $t_g = 0s$ , thrust  $F = 2N$ , and specific impulse  $I_{sp} = 200s$ . The simulation neglects the impact of target's pulse maneuver on its mass

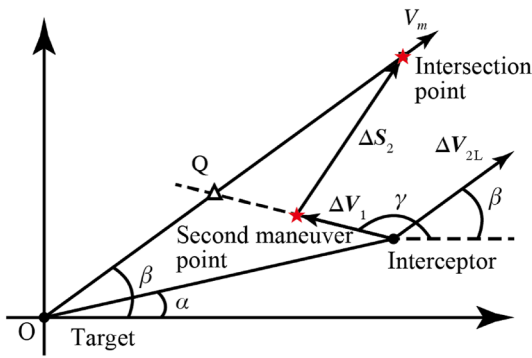


Fig. 5 Interception Maneuver analysis diagram

and excludes perception and decision-making time. The calculated duration for completing the interception mission is 1865s, as shown in Figs. 2, 3 and 4.

Figure 2 illustrates that when the interceptor satellite with zero initial velocity, its first segment trajectory is linear while the second segment follows a curved path. Figure 4 further reveals that during the mission, changes in distance between interceptor and target occur at different rates along components parallel and perpendicular to target’s velocity direction. The difference between them experiences uniform acceleration followed by deceleration perpendicular to target’s velocity direction; however, only in the second segment does it gradually reduce their speed differential along target’s velocity direction, providing clearer insight into the maneuver strategy adopted by this interception plan.

### 3 Multi-satellite Pursuit Configuration Design

#### 3.1 Existence Analysis of Planar Interception Task Solutions

##### 3.1.1 Existence Analysis of Task Solutions

Before designing the multi-satellite pursuit configuration, it is necessary to determine under what conditions a feasible solution exists for the interception task. The maneuvering process for planar interception is illustrated in Fig. 5. Firstly, for the first maneuver azimuth angle  $\gamma$ , in order for the above problem to have a solution, it is required that  $\Delta V_1$  lies between  $-R$  and  $V_m$ .

Considering the decomposition of the second maneuver displacement vector, the entire maneuver process can also be re-decomposed as:

- (1) Along  $\Delta V_1$ : one-dimensional acceleration/deceleration phase
- (2) Along  $\Delta V_{2L}$ : one-dimensional acceleration phase

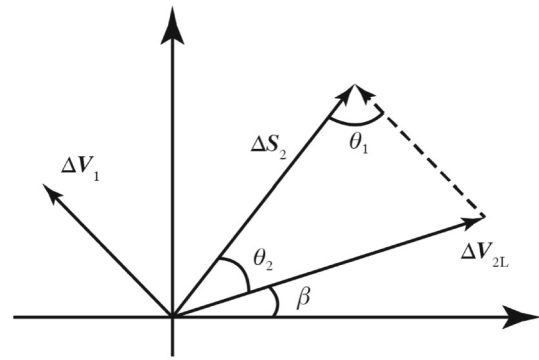


Fig. 6 Non-orthogonal decomposition of second displacement segment

The displacement along direction during these two maneuvers can be expressed as:

$$|S_{\Delta v_{1ad}}| = |\Delta S_1| + |\Delta S_{\Delta v_{1d}}| \tag{16}$$

Where point Q is the intersection point between  $\Delta V_1$  direction and target motion direction.

The direction pointing from initial position of interceptor satellite towards Q point is represented by:

$$\rho = R + \Delta V_1 \cdot l_1 \quad l_1 \geq 0 \tag{17}$$

Where direction OQ represents:

$$\rho = V_m \cdot l_2 \quad l_2 \geq 0 \tag{18}$$

Solving the above equations gives us:

$$l_2 = \frac{R(\sin \alpha - \tan \gamma \cos \alpha)}{v_m(\sin \beta - \tan \gamma \cos \beta)} \tag{19}$$

Thus, distance between initial position of interceptor satellite and Q point can be expressed as:

$$L_{IQ} = \|OQ - R\|_2 \tag{20}$$

where:

$$OQ = \begin{bmatrix} \frac{R(\sin \alpha - \tan \gamma \cos \alpha)}{\tan \beta - \tan \gamma} \\ \frac{R \tan \beta (\sin \alpha - \tan \gamma \cos \alpha)}{\tan \beta - \tan \gamma} \end{bmatrix}$$

$$R = \begin{bmatrix} R \cos \alpha \\ R \sin \alpha \end{bmatrix}$$

Notice that  $|S_{\Delta v_{1ad}}|$  depends on  $\Delta v_1$  and  $\gamma$ , given any value of  $\gamma$ , letting  $|S_{\Delta v_{1ad}}| = L_{IQ}$  will yield corresponding  $\Delta v_1$ . From equation (11), we obtain  $\gamma$  which corresponds to interception time for first maneuver azimuth angle.

On line OQ, we have the displacement components of the target and interceptor as follows:

$$\begin{aligned} L_T(t) &= v_m t \\ L_I(t) &= \|\mathbf{OQ}\|_2 + L_{\Delta v_{2L}} \end{aligned} \tag{21}$$

where  $\|\mathbf{OQ}\|_2$  can be obtained from equation (19), and both  $|\Delta \mathbf{S}_{\Delta v_{1d}}|$  in equation (16) and  $L_{\Delta v_{2L}}$  in equation (21) are derived from non-orthogonal decomposition of  $\Delta \mathbf{S}_2$ . See Fig. 6.

Noting that  $\Delta \mathbf{S}_2$  must lie between  $\Delta \mathbf{V}_1$  and  $\Delta \mathbf{V}_{2L}$ , according to sine theorem we have:

$$\frac{|\Delta \mathbf{S}_2|}{\sin(\pi - \theta_1 - \theta_2)} = \frac{|\Delta \mathbf{S}_{\Delta v_{1d}}|}{\sin \theta_2} = \frac{L_{\Delta v_{2L}}}{\sin \theta_1} \tag{22}$$

where:

$$\begin{aligned} \theta_1 &= \arccos\left(\frac{\Delta \mathbf{S}_2 \cdot \Delta \mathbf{V}_1}{|\Delta \mathbf{S}_2| |\Delta \mathbf{V}_1|}\right) \\ \theta_2 &= \arccos\left(\frac{\Delta \mathbf{S}_2 \cdot \mathbf{V}_m}{|\Delta \mathbf{S}_2| |\mathbf{V}_m|}\right) \end{aligned}$$

Let us denote  $f = L_I(t) - L_T(t)$  as a function representing the interception capability margin of the interceptor satellite. If  $f \geq 0$ , then the interceptor has interception capability at angle  $\gamma$ .

### 3.1.2 Simulation Case Study of Planar Interception Range

Considering a planar interception problem with a specified time limit, the azimuth angle range that an intercepting satellite can intercept under the given constraints is determined. Given a time threshold  $T = 1800$  s (limiting the distance of target maneuver, i.e., the expected total fuel threshold); fixed target velocity direction  $\beta = 0^\circ$ , with speed  $v_m = 5$  m/s; interceptor initial velocity at 0, initial distance  $R = 20,000$  m, coasting time  $t_g = 0$  s, thrust  $F = 2N$ , specific impulse  $I_{sp} = 200$  s, one can obtain the range of interceptor azimuth angles  $\alpha \in (0, \pi)$  that satisfy the aforementioned interception requirements and interceptor capabilities, i.e., providing the maximum range  $\alpha_{\max}$  that an intercepting satellite can cover.

Figure 7 depicts the relationship between intercepting satellite azimuth and feasible angular ranges  $\gamma$ , showing that for an intercepting satellite to be feasible, its initial position should be near  $\mathbf{V}_m$ . The smaller deviation results in a larger feasible  $\gamma$  range. This problem is symmetric when  $\alpha \in (\pi, 2\pi)$ , and yields feasible ranges for initial azimuths of an intercepting satellite  $\alpha_{\max} = 104.88^\circ$ ; subsequently determining that to achieve orbital blockade on a plane after specifying parameters such as distance from target and inter-

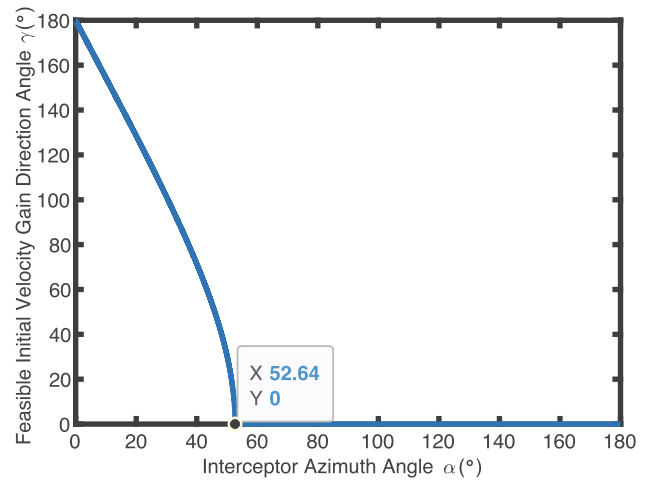


Fig. 7 Initial azimuth of intercepting satellite  $\alpha$ —effective initial velocity direction angle  $\gamma$

ceptor maneuverability, at least four intercepting satellites are required.

## 3.2 Design of Planar Interception Configuration under Elliptical Passive Flyby Conditions

### 3.2.1 Passive Flyby Theory

The interception problems mentioned above are all based on the inference that the intercepting satellite is stationary relative to the coordinate system. Now, let's consider a passive flyby of the intercepting satellite formed relative to the target satellites.

The analytical solution of CW equation in the X-Y plane is:

$$\begin{aligned} x &= \left(\frac{4\dot{x}_0}{\omega} + 6y_0\right) \sin \omega t + \frac{2\dot{y}_0}{\omega} \cos \omega t \\ &\quad - (3\dot{x}_0 + 6\omega y_0)t + x_0 - \frac{2\dot{y}_0}{\omega} \\ y &= -\left(\frac{2\dot{x}_0}{\omega} + 3y_0\right) \cos \omega t + \frac{\dot{y}_0}{\omega} \sin \omega t + \frac{2\dot{x}_0}{\omega} + 4y_0 \end{aligned} \tag{23}$$

Under passive flyby conditions  $3\dot{x}_0 + 6\omega\dot{y}_0 = 0$ , let:

$$\begin{aligned} A &= \frac{2\dot{x}_0}{\omega} + 3y_0 \\ B &= \frac{-\dot{y}_0}{\omega} \end{aligned} \tag{24}$$

Equation (23) can be written as follows:

$$\frac{(x - x_c)^2}{4(A^2 + B^2)} + \frac{(y - y_c)^2}{A^2 + B^2} = 1 \tag{25}$$

where,

$$x_c = x_0 - \frac{2\dot{y}_0}{\omega}$$

$$y_c = \frac{2\dot{x}_0}{\omega} + 4y_0$$

Assuming that the center point of elliptical flyby coincides with the target satellite (i.e., origin), then equation (23) can be rewritten as:

$$x = x_0 \cos \omega t$$

$$y = \frac{1}{2}x_0 \sin \omega t \tag{26}$$

The velocity expression is given by:

$$\dot{x} = -x_0\omega \sin \omega t$$

$$\dot{y} = \frac{1}{2}x_0\omega \cos \omega t \tag{27}$$

Thus, given a target satellite orbit height  $R_T$ , intercepting satellite's semi-major axis of elliptical companion flight  $a$ , and intercepting satellite azimuth angle  $\alpha$ , we can uniquely determine the current position and velocity vector of the intercepting satellite in relative coordinates. With reference to the intercepting satellites, the speed of the target satellite becomes  $\mathbf{V}_m - \mathbf{V}_{int}$  so that we can transform this problem into one where initial speed of intercepting satellites is 0, making it easier to draw conclusions about situations involving elliptical flybys.

### 3.2.2 Elliptical Flyby Simulation Case Study

In the scenario of elliptical flybys, the angle range within which an intercepting satellite can intercept a target satellite within a specified time limit is recalculated. Assuming the target satellite is in GSO with an orbital radius  $R = 4.2164 \times 10^7$  m, and given a interception mission time threshold (limiting the distance of target maneuver)  $T = 1800$  s (which is equivalent to limiting fuel threshold when  $t_g = 0$  s). The maneuver velocity increment  $v_m = 5$  m/s. The interceptor is located on the elliptical path around the target satellite, satisfying passive flyby conditions. With an elliptical semi-major axis  $a = 20,000$  m, coasting time  $t_g = 0$ , thrust  $F = 2$  N, specific impulse  $I_{sp} = 200$  s, for each interceptor azimuth angle  $\alpha \in (0, \pi)$  corresponding to meeting interception conditions, there exists an angular range of  $\beta$  (the problem exhibits periodicity with  $\alpha$  as a period of  $\pi$ ).

As shown in Fig. 8, under this simulation scenario with an elliptical passive flyby condition and a semi-major axis of 20,000m, the relationship between the position of the intercepting satellite and possible escape directions for the target satellite are obtained. The minimum interceptable escape

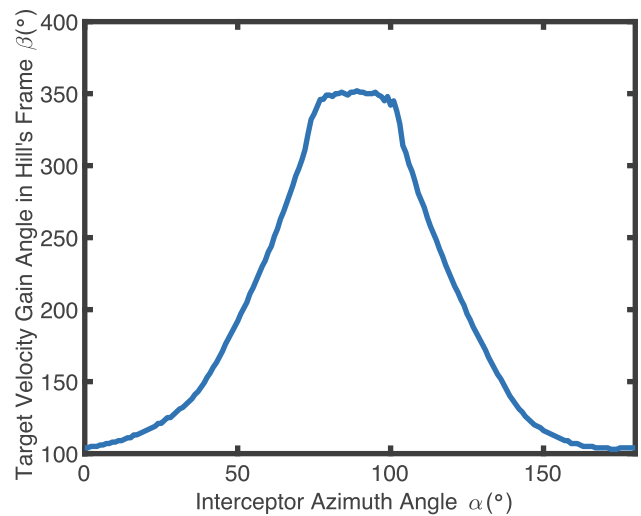


Fig. 8 Interceptor azimuth angle under elliptical passive flyby  $\alpha$ —meeting interception conditions for target satellite velocity gain angle  $\beta$

direction is at  $104^\circ$ . Therefore, under satisfying elliptical passive flyby conditions, at least four interceptors are required in one interception plane to completely block off that escape plane. Each satellite distributes evenly around the target satellite forming a passive flyby blockade configuration.

## 4 Simulation and Analysis

### 4.1 Simulation of Planar Interception Problem

The initial velocity of the target satellite and the initial distance between the intercepting satellite and the target satellite will significantly affect the interception capability of a single satellite. In this section, based on the setup and parameters of the planar interception problem in Sect. 3.1.2, simulations are conducted to calculate feasible interception azimuth angles for a single interceptor.

#### 4.1.1 Influence of Target Satellite's Initial Velocity on Planar Interception

The initial velocity of the target satellite, representing its maximum maneuverability, determines the difficulty level of interception for an interceptors. The stronger the maneuverability of the target, the greater cost it incurs for an interceptor to achieve interception. In the planar interception problem described in Sect. 3.1.2, by varying the initial velocity of the target, feasible interception azimuth angle ranges for an interceptor are illustrated in Fig. 9.

From Fig. 9, it can be observed that when the initial velocity of the target is less than 10m/s, the feasible range of change in interception azimuth for the interceptor is rela-

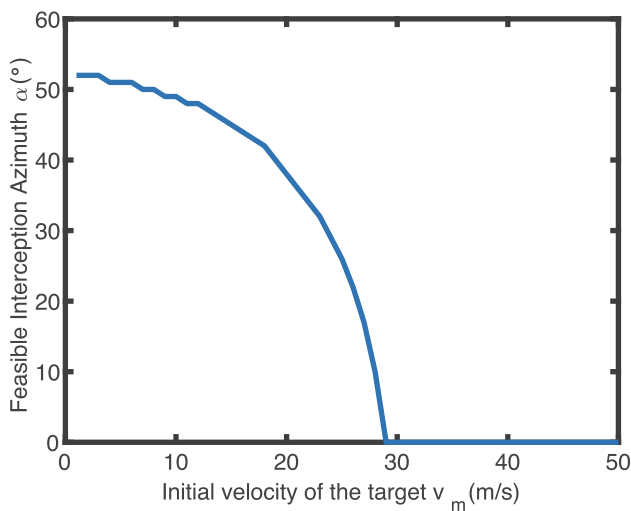


**Fig. 9** Influence of target's initial velocity on feasible interception azimuth angles

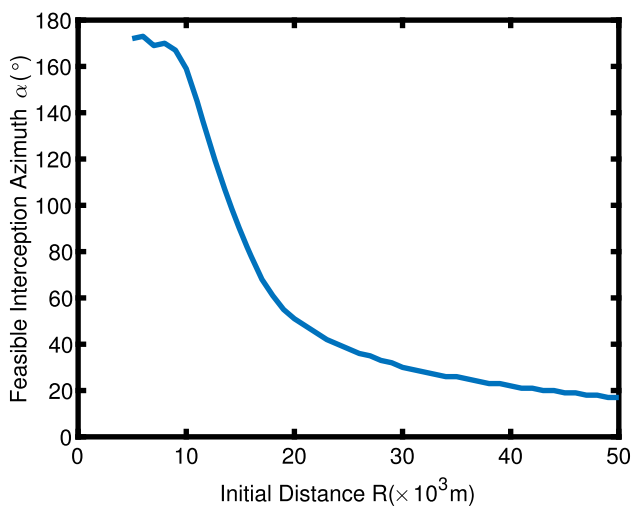


**Fig. 10** Influence of initial intercept distance on feasible intercept azimuth angles

tively small. This implies that deploying four interceptors can effectively block the target. As the velocity of the target satellite further increases, the feasible azimuth angle for a single interceptor decreases sharply, necessitating more interceptors to ensure interception within a specified time frame. When the velocity of the target exceeds 29 m/s, interception cannot be achieved within a designated time period.

#### 4.1.2 Influence of Initial Distance on Planar Interception

In multi-satellite interception scenarios, the initial distance between the interceptor and target is manifested as the flyby radius. A larger flyby radius results in a longer total distance traveled during the interception process. In Sect. 3.1.2's planar interception problem, varying the initial

distance between the interceptor and target defines feasible intercept azimuth angles for the interceptor as shown in Fig. 10.

The results show that when the distance from the interceptor to the target exceeds 10,000 m, the feasible range of azimuth angles for a single interceptor rapidly decreases with increasing initial distance. The maneuver time required for the planar interception strategy proposed in this paper significantly increases, indicating greater fuel consumption. When the initial distance between the interceptor and target satellite reaches 50,000 m, the feasible azimuth angle for the interceptor is only 17°. At this point, it is necessary to deploy 11 interceptors in order to complete interception within a specified time frame.

## 4.2 Elliptical Multi-satellite Pursuit-Evasion Simulation

Building upon the planar interception strategy in Sect. 2.2.2 and the elliptical passive circumnavigation configuration in Sect. 3.2.2, this section conducts a simulation case study on the interception of multiple interceptor targeting a single satellite within the orbital plane of GSO, using simulation parameters consistent with those in Sect. 3.2.2. Considering that both the interceptor and the target are GSO satellites, with the primary difference being that the interceptor's orbit has a smaller eccentricity, the angular velocity of the interceptor relative to the target on the passive circumnavigation ellipse can be approximated as constant. In this paper, the interceptor satellites are evenly distributed along the passive circumnavigation ellipse of the target satellite, starting from the positive X-axis and numbered counterclockwise, with interceptor 1 at an initial phase angle. Each interceptor will maintain equal angular spacing during the circumnavigation.

### 4.2.1 Multi-satellite Pursuit-Evasion Simulation

Assuming that four interceptors form an elliptical passive circumnavigation encirclement configuration around the target, when interceptor 1 reaches a phase angle, the target maneuvers towards a direction at a phase angle of 35° to escape with maximum maneuverability until one of the interceptors successfully completes its mission and terminates pursuit operations. In this scenario, interceptor 2 is first to complete its interception task; at this point, as shown in Fig. 11, all four interceptors' trajectories during interception are illustrated, taking a total time of 1558s.

Figures 12 and 13 depict changes in distance and velocity differentials between each interceptor and the target throughout their respective interceptions: it can be observed that each interceptor gradually reduces its distance from the target during pursuit operations while achieving successful encirclement; furthermore, overall velocity differentials exhibit



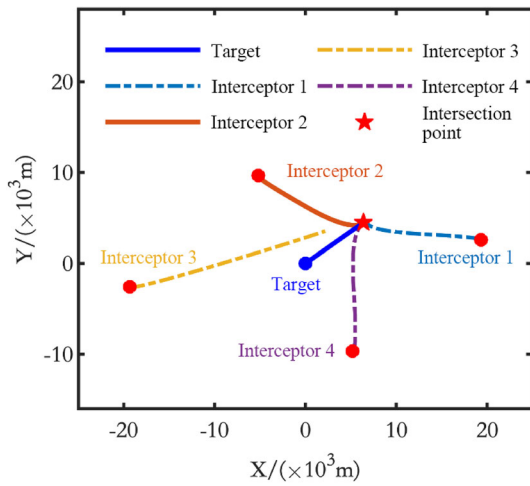


Fig. 11 Interceptors' trajectories

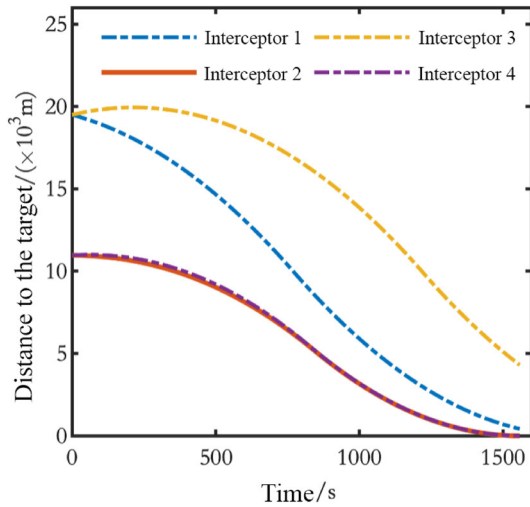


Fig. 12 Distance between each interceptor and target

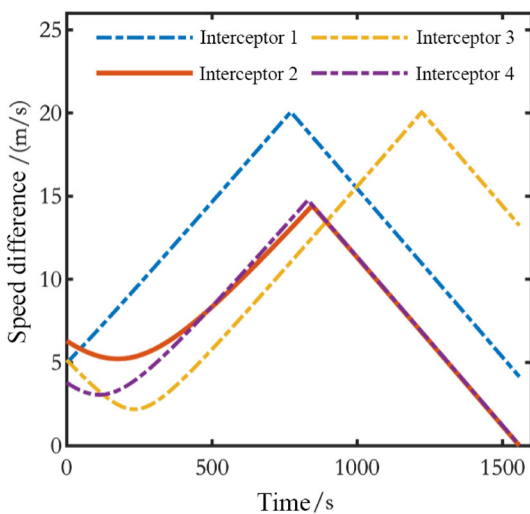


Fig. 13 Velocity differential between each interceptor and target

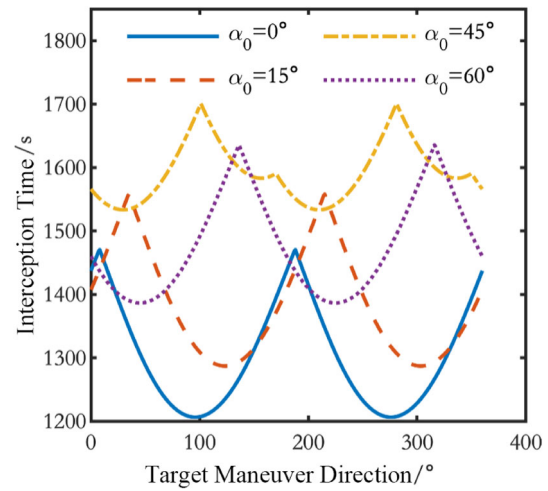


Fig. 14 Interception times for configuration with four interceptors

an increasing-then-decreasing trend similar to characteristics seen in one-on-one planar interceptions cases but differ due to initial velocities possessed by interceptors leading to distinctions compared to early stages of one-on-one planar interceptions.

#### 4.2.2 Impact of Target Maneuver Direction on Pursuit

The escape direction of the target significantly affects the time required for interception missions. Under a configuration with four interceptors, the interception times for each interceptor are calculated, and the time taken by the interceptor that completes the task first is considered as the total mission interception time. By altering the escape direction of the target, simulations are conducted in scenarios where interceptor 1's phase angle is set at 0°, 15°, 45°, and 60° respectively to determine the required interception times as shown in Fig. 14.

From Fig. 14, it can be observed that changes in the maneuver direction of the target will cause fluctuations in the required interception time (i.e., fuel consumption). In this section, when the phase angle of interceptor 1 is 0°, the interception time varies minimally with changes in the maneuver direction of the target; when the phase angle of interceptor 1 is 45°, the interception time varies maximally with changes in the maneuver direction of the target. Combining with Fig. 10, it is not difficult to find that when the phase angle of interceptor 1 is 0°, there is a maximum difference in distances between each interceptor and the target, while at a phase angle of 45°, all interceptors are equidistant from the target. The differences in distance result in variations in interception duration.

Furthermore, each inflection point on every curve in Fig. 14 signifies a change in which interceptor completes its mission. When interceptor 1 has a phase angle of 45° and all

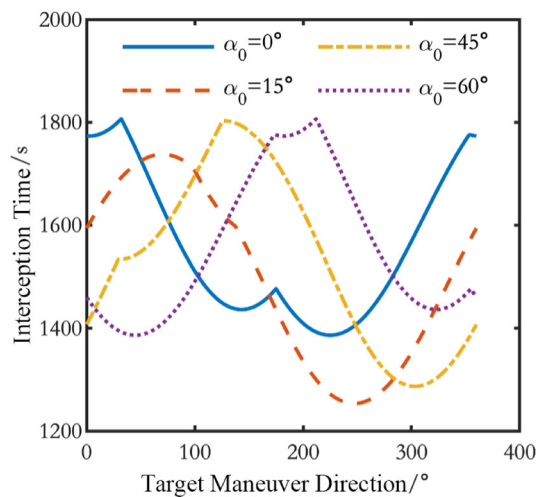


**Fig. 15** Interception times for three-interceptor configuration

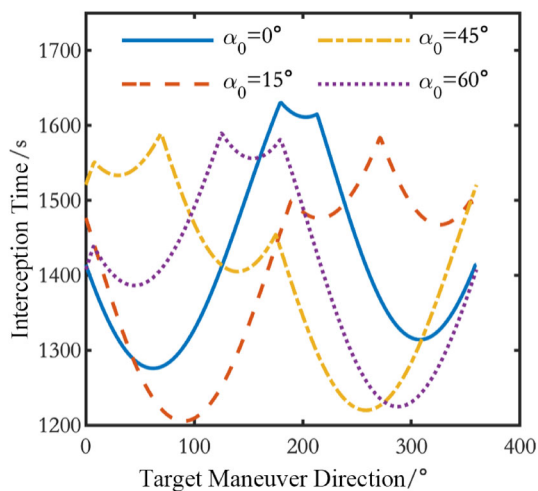


**Fig. 16** Interception times for five-interceptor configuration

four interceptors are equidistant from the target satellite, any one of them could potentially become an optimal interceptor as changes occur in maneuver direction. However, under other circumstances where there are significant differences in distances to reach their targets, typically it is easier for an interceptor closest to its target to complete an interception task successfully; during such instances only two inflection points appear on curves.

#### 4.2.3 Impact of Interceptor Number on Capture

Under the conditions of elliptical passive flyby, the angular difference between each interceptor does not change with time. When interceptors are evenly distributed around the target satellite in one orbit, the capture configuration becomes denser as the number of interceptors increases. Simulations were conducted for scenarios with configurations of 3 and 5 interceptors, where interceptor 1's phase angles were set

at  $0^\circ$ ,  $15^\circ$ ,  $45^\circ$ , and  $60^\circ$  respectively to obtain the required interception times as shown in Figs. 15 and 16.

Comparing the results from Figs. 14, 15 and 16 reveals that as the number of interceptors increases, the maximum mission duration decreases accordingly. In the three-interceptor configuration results shown in Fig. 15, there are multiple instances where total mission duration exceeds the designated limit of 1800 s during configuration design; this validates that a minimum of four interceptors is needed to achieve interception tasks under specified conditions in this study. Considering both initial distance between interceptors and target satellite's impact on interception tasks, configurations with more interceptors can bring them closer to their target satellite during maneuvers to avoid weak links appearing throughout flybys.

## 5 Conclusion

In this study, the method for solving the planar rapid interception problem was derived using Tsiolkovsky's formula, and criteria were proposed for designing multi-satellite encirclement configurations under elliptical formation flying conditions. Through simulation experiments, the impact of the initial velocity magnitude of the target satellite and the initial distance between interceptor and target satellites on planar interception tasks was investigated. Furthermore, the interception effectiveness against target maneuvers in any direction under different configurations was explored. The research results validated the design method of planar interception configurations under elliptical passive formation flying conditions, providing technical support for solving satellite maneuvering pursuit configuration design problems in continuous propulsion mode.

Several aspects for further research are identified in this study:

- (1) Configuration design methods in three-dimensional scenarios;
- (2) Interception strategy design for long-distance interception tasks;
- (3) Design of multi-round interception strategies and configurations.

**Acknowledgements** This research was supported by the National Natural Science Foundation of China (Grant Number: NFSC20200090); and the Basic Strengthening Project of Military Science and Technology Commission (Grant Number: JZKJW20210031). We are grateful to the editor and reviewers for their feedback, which helped us improve our manuscript.

**Author Contributions** Weike Wang: conceptualization, methodology, investigation, writing; Hanjun Wang: methodology, investigation, writing; Tian Liao: methodology; Shunli Li: supervision; Mengping Zhu: supervision, conceptualization.

**Funding** This work was supported by the National Natural Science Foundation of China (Grant number: NFSC20200090); and the Basic Strengthening Project of Military Science and Technology Commission (Grant number: JZKJW20210031).

**Data Availability** The data underlying this article will be shared on reasonable request to the corresponding author.

## Declarations

**Conflict of interest** Professor Shunli Li is a guest editor for the special issue "Spacecraft Orbital Game".

**Ethical approval** This article does not contain any studies with human participants or animals performed by any of the authors.

**Informed consent** For this type of study formal consent is not required.

## References

- Liao T, Li S, Chen X, Zhu M (2023) Numerical solution of spacecraft pursuit-evasion-capture game based on progressive shooting method. *Proc Inst Mech Eng Part G J Aerosp Eng*. <https://doi.org/10.1177/09544100231164269>
- Luo Y, Zhu H, Li Z (2020) Survey on spacecraft orbital pursuit-evasion differential games (in Chinese). *Scientia Sinica Technologica* 50(12):1533–1545. <https://doi.org/10.1360/SST-2019-0174>
- Zy Li, Zhu H, Yang Z, Luo YZ (2019) A dimension-reduction solution of free-time differential games for spacecraft pursuit-evasion. *Acta Astronautica* 163:201–210. <https://doi.org/10.1016/j.actaastro.2019.01.011>
- Liao T (2021) Research on control and solving method of pursuit-evasion game for spacecraft (in Chinese) [Master's Thesis]. Harbin Institute of Technology, Harbin
- Zeng X, Cai W, Yang L, Zhu Y (2018) On the orbital pursuit-evasion games with low constant thrust-to-mass ratio. In: 2018 Chinese automation congress (CAC), pp 1655–1660. <https://ieeexplore.ieee.org/document/8623543/>
- Ye D, Shi M, Sun Z (2018) Satellite proximate interception vector guidance based on differential games. *Chin J Aeron* 31(6):1352–1361. <https://doi.org/10.1016/j.cja.2018.03.012>
- Zhu H (2017) Optimal control of spacecraft orbital pursuit-evasion based on differential game (in Chinese) [Master's Thesis]. National University of Defense Technology, Changsha
- Li Z, Zhu H, Luo Y (2021) An escape strategy in orbital pursuit-evasion games with incomplete information. *Sci China Technol Sci* 64(3):559–570. <https://doi.org/10.1007/s11431-020-1662-0>
- Zhu H, Luo YZ, Li ZY, Yang Z (2019) Orbital pursuit-evasion games with incomplete information in the hill reference frame. In: Proceedings of 27th international symposium on space flight dynamics (ISSFD). Melbourne, pp 1–6
- Zhou J (2021) Research on control method for spacecraft pursuit-evasion based on differential game theory (in Chinese) [PhD thesis]. Harbin Engineering University, Harbin
- Chen M (2021) Solving the pursuit-evasion strategies of three spacecrafts based on differential game and coevolution algorithm (in Chinese) [Master's Thesis]. Harbin Institute of Technology, Harbin
- Liu Y, Li R, Hu L, Cai ZQ (2018) Optimal solution to orbital three-player defense problems using impulsive transfer. *Soft Comput* 22(9):2921–2934. <https://doi.org/10.1007/s00500-017-2545-3>
- Shirobokov M, Trofimov S, Ovchinnikov M (2021) Survey of machine learning techniques in spacecraft control design. *Acta Astronautica* 186:87–97. <https://doi.org/10.1016/j.actaastro.2021.05.018>
- Geng Y, Yuan L, Huang H, Tang L (2023) Terminal-guidance based reinforcement-learning for orbital pursuit-evasion game of the spacecraft (in Chinese). *Acta Automatica Sinica* 49(5), 974–984. <https://doi.org/10.16383/j.aas.c220204>
- Yuan L, Geng Y, Tang L, Huang H (2022) Multi-stage reinforcement learning method for orbital pursuit-evasion game of spacecrafts (in Chinese). *Aerosp Shanghai (Chinese & English)* 39(4):33–41. <https://doi.org/10.19328/j.cnki.2096-8655.2022.04.003>
- Li B, Yue K, Gan Z, Gao P (2021) Multi-UAV cooperative autonomous navigation based on multi-agent deep deterministic policy gradient (in Chinese). *J Astron* 42(6):757–765
- Shi W, Feng Y, Cheng G, Huang H, Huang J, Liu Z et al. (2021) Research on multi-aircraft cooperative air combat method based on deep reinforcement learning (in Chinese). *Acta Automatica Sinica* 47(7), 1610–1623. <https://doi.org/10.16383/j.aas.c201059>
- Zhao L, Zhang Y, Dang Z (2023) PRD-MADDPG: an efficient learning-based algorithm for orbital pursuit-evasion game with impulsive maneuvers. *Adv Space Res* 72(2):1709–1720. <https://doi.org/10.1016/j.asr.2023.03.014>

Springer Nature or its licensor (e.g. a society or other partner) holds exclusive rights to this article under a publishing agreement with the author(s) or other rightsholder(s); author self-archiving of the accepted manuscript version of this article is solely governed by the terms of such publishing agreement and applicable law.